Chapter 2: Multimode Analysis of Conventional Gyro-twystron Amplifier*

2.1 Introduction

2.2 Design Methodology of Gyro-twystron

2.2.1 Interaction Structure Design

2.2.2 Beam Present Design Issues

2.3 Multimode Analysis of Gyro-twystron

2.4 Numerical Benchmarking

2.5 Conclusion

*Part of this work has been published as:

Anshu S. Singh, S. Yuvaraj and M. Thottappan, "Analytical and PIC Simulation Studies of a Megawatt Class Gyrotwystron Amplifier," *IEEE Transactions on Electron Devices*, vol. 63, no. 10, pp. 4104-4112, Oct. 2016.

2.1 Introduction

The development of microwave tubes up to the gyro-twystron is discussed in the previous chapter along with their physics and classification. CRM devices with their operating principle are discussed in more depth and lead us to gyro-twystron review. However, Literature surveys of gyro-twystron are bounded to report the performance metrics, scope and limitation. Analytical model and mathematical formalism of gyro-twystron are discussed in the present chapter. Development of design methodology and the nonlinear theory for beam-wave interaction are the objective of this chapter.

Pre-bunching RF section and output waveguide section of gyro-twystron is similar to gyro-klystron and gyro-TWT, respectively, which are reflected in existing mathematical formalism. Various design techniques are imported from the parental gyro-amplifiers of gyro-twystron and literature of gyro-amplifiers are restructured to develop a design methodology of gyro-twystron. In 1985, Chu *et al.* developed a design methodology for the megawatt-class gyroklystron amplifier, and the choice of operating mode, frequency, wall loss and space charge effects are incorporated in the design studies. Later on, in 2000 several gyroklystron tubes are designed using the MAGYKL code, which is the extended version of gyrotron design code MAGY. As compared to gyro-klystron, gyro-TWT has simpler interaction structure, i.e. cylindrical waveguide. However, the operation of gyro-TWT is complex and vulnerable to the oscillations, which are caused by both external and internal feedback mechanisms. Therefore, the design of RF interaction structure with stability is a major constraint in gyro-TWT. Reflections cause external feedback driven oscillations from the output power extraction system and an internal feedback mechanism. The operating characteristics of gyro-TWT are discussed through the dispersion curve to ensure the region of convective instability as well as to identify the backward wave modes to investigate the absolute instability. The

critical length calculation of backward wave modes is essential for designing gyro-TWT, as the waveguide length is kept smaller than the critical length of backward wave modes for stable operation. With these design methodologies advancements in gyroklystron and gyro-TWT, we have derived and developed design methodology of gyro-twystron.

2.2 Design Methodology of Gyro-twystron

The design methodology of gyro-twystron is governed by principle and physics of VEDs. Electromagnetic behaviour of each component of gyro-twystron has been studied in the presence/absence of electron beam to develop the design methodology including the choice of the desired mode, electron beam parameters, and operating the magnetic field. Desired goals and performance metrics motivate the design methodology, as these data are initial input for design calculations. In the first step, the calculation of RF dimension has been done to support the desired mode and frequency of an electromagnetic wave. In the second step, electron beam parameters are incorporated in design calculations, e.g. start oscillation current is a function of quality factor. Stability analysis of field carrying interaction structures such as cavity and waveguide has been done to operate below start oscillation current. Design a hybrid interaction structure for beam-wave interaction is tedious and to simplify the design approach each section of gyro-twystron is designed independently. Drift tubes are designed to provide isolation between cavities and waveguide. Detail of design methodology of each section is discussed as follows.

2.2.1 Interaction structure design

2.2.1.(a) Input cavity

The radius of the RF structure depends upon frequency of operation and operating mode. The radius of the input cavity is chosen such that the cut-off frequency is lower than operating frequency for an operating mode. The cavity cut off radius r_{cav} for TE_{mn} mode is given by,

$$r_{cav} = x_{mn}\lambda / 2\pi \tag{2.1}$$

where, x_{mn} is Eigen value of TE_{mn} mode, and λ is the wavelength of RF input signal. Resonating frequency (f_r) of TE_{mnd} mode in a circular cavity is determined by

$$f_r = \left(\frac{c}{2\pi}\right)\left(\sqrt{\left(x_{mn}/r_{cav}\right)^2 - \left(d\pi/L_c\right)^2}\right) \tag{2.2}$$

The length and radius of the cavity are optimized to achieve the desired resonating frequency. Short length overmoded cavities are designed to reduce the space charge effect and hold the constraint of the point gap model. Resonating frequency of unloaded cavity is kept slightly higher as the dielectric loading decreases the resonating frequency. The dielectric loading is introduced to the cavity to reduce the quality factor and increase the start oscillation current (I_{soc}).

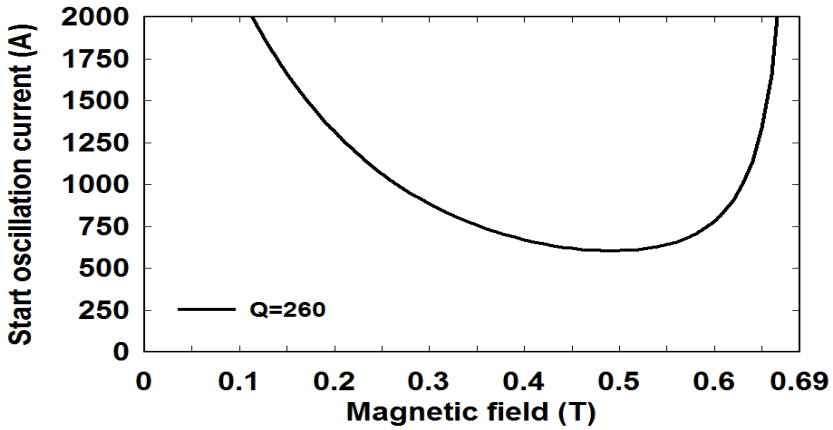

Figure 2.1. SOC of the input cavity of gyro-twystron

For stable operation, the beam current is kept lower SOC of the cavity, which is calculated by the following expression

$$I_{s_{cav}} = \left(\frac{\pi}{2}\right)^{5/2} \frac{c^3 m_e \varepsilon_0}{e}\left(\frac{2^s s!}{s^s}\right)\frac{\beta_{t0}^{-2(3-s)}\gamma_0}{Q}\frac{L_c}{\lambda}\frac{(4/\pi\mu^2)[e^{2x^2}/(\mu x - s)]}{H_{mn}} \tag{2.3}$$

To allow the high current operation, the cavity is loaded to achieve the quality factor below 500. For reducing the initial oscillations in the RF output power, the quality factor

of the input cavity is lowered by loading with a lossy dielectric material. Figure 2.1 shows input cavity with the quality factor of 260 possess the SOC above to 600 A for magnetic field range from 0.3 T to 0.6 T. Apart from the dielectric loading, the input cavity is designed to optimize the complex gain function, which is a measure of the susceptibility of the electron beam to the RF wave.

2.2.1. (b) Drift tube

The field free drift tube is designed to provide isolation between cavity and waveguide. The radius of the drift section is chosen to provide cut-off to RF operating frequency but should not be minimised beyond the beam radius to avoid beam-interception with drift tube walls. To provide the isolation between adjacent cavities and waveguide, the length of the drift tube is chosen by cold cavity dispersion relation. The radius of the drift section is determined by the following inequalities,

$$r_d < x_{mn}\lambda / 2\pi \text{ , and } r_b < r_d < r_{cav}, r_{w\ \min}, \tag{2.4}$$

The length of the drift tube is chosen to provide the isolation by the cold cavity dispersion relation

$$L_d > 5.75 \Big/ \left[x_{mn}/r_d{}^2 - \omega/c{}^2 \right]^{1/2}. \tag{2.5}$$

For high power operation, TE_{11} mode is not suitable as the transverse dimension is smaller which leads to beam interception in the drift tube. The TE_{01} mode has eigenvalue of 3.831 almost double to TE_{11} mode and provides a larger transverse dimension to not only reduces space charge effect and beam interception but also lowers wall loss through azimuthal symmetry. To cut-off the operating TE_{01} mode, TE_{21} as the immediate lower mode is chosen. To suppress the TE_{11} mode, the drift tube is heavily loaded with the dielectric rings and length of drift tube is increased. The loading near to the cavity-drift tube junction further reduces the quality factor, and dielectric rings are loaded to drift tubes away from the end of the cavity.

2.2.1.(c) Output waveguide section

The length of the output waveguide is decided by the minimum value of the beam current at which the oscillation starts. Oscillations in gyro-travelling wave amplifiers arise due to the internal feedback mechanism of absolute instability. Beam wave interaction operation in gyro-travelling wave amplifiers is based on convective instability. However, at higher current, these convective instability turns into absolute instability. Beam parameters are chosen carefully to avoid the absolute instability. Absolute instability is investigated by the dispersion equation,

$$\left(\omega^2 - c^2\left(k_z^2 + k_{mn}^2\right)\right)\left(\omega - k_z v_z - s\Omega/\gamma\right)^2 = -\varepsilon_c . \tag{2.6}$$

$$\text{where,} \quad \varepsilon_c = \frac{4\beta_t^2 I\left(J_{m\pm s}\left(k_t r_g\right)*\left(J_n^{'}\left(k_t r_L\right)\right)\right)^2}{\gamma_o \beta_z I_A\left(x_{mn}^2 - m^2\right)J_m^2\left(x_{mn}\right)}$$

ω is angular frequency, k_z is the axial wave number, $k_{mn} = x_{mn}/r_w$, x_{mn} is the n^{th} root of $J_m^{'}\left(x_{mn}\right) = 0$, β_{t0} is initial normalized transverse velocity component, I_b is beam current, $I_a \approx 17\beta_{zo}\gamma_0$ kA is Alfven current, $\gamma_0 = \left(1-\beta_z^2-\beta_t^2\right)^{-1/2}$, $\Omega = eB_0/m_e$, r_w, r_g and r_L are wall radius, guiding centre radius and Larmor radius, respectively, and

$$L_{wg}^3 = \frac{15.82\beta_z^2 k_z \gamma_o \beta_z I_A\left(x_{mn}^2 - m^2\right)J_m^2\left(x_{mn}\right)}{4\beta_t^2 I\left(J_{m\pm s}\left(k_t r_g\right)*\left(J_n^{'}\left(k_t r_L\right)\right)\right)^2 k_t^4} \tag{2.7}$$

Current *(I)* is inversely proportional to cubic of critical length *(L)* of the waveguide, and above the critical length at which backward wave oscillation starts. For stable operation, the pitch factor of the electron beam is upper bounded as $L_{wg}^3 \propto \beta_z^3/\beta_t^2$. Figure 2.2 shows that SOC decreases as the length of waveguide increases.

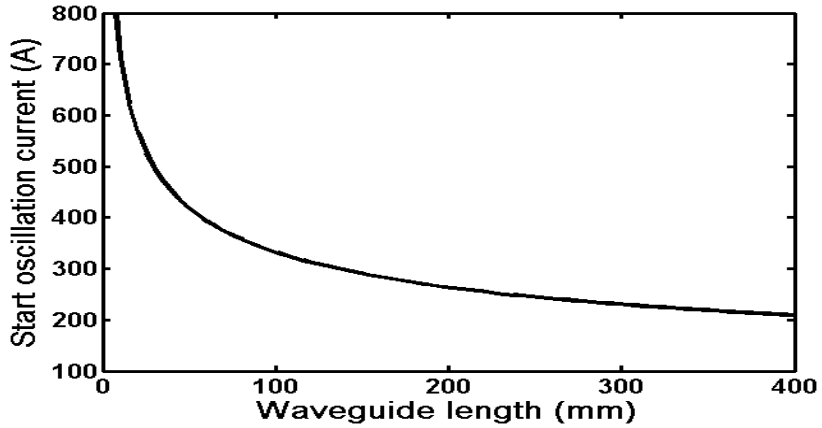

Figure 2.2 Start oscillation current Vs waveguide length unloaded gyro-twystron

2.2.2 Beam present design issues

The magnetic field governs the cyclotron frequency of particles for the beam wave interaction and the synchronism between the electron beam and operating frequency is governed by CRM mechanism,

$$\omega - k_z v_z = s\Omega / \gamma \tag{2.8}$$

Where, $\Omega = (e/m_e) * B_0$ and by ignoring the Doppler shift term ($k_z v_z$), the magnetic field (B) for CRM mechanism is determined by following expression,

$$B_0 \sim \frac{2\pi f}{s\left(e/\gamma m_e\right)} \tag{2.9}$$

The requirement of the magnetic field is dependent on the operating frequency, which is in the order of product of cyclotron frequency and beam mode harmonic number. DC input beam parameters are calculated using the desired efficiency and RF power. The electronic efficiency (η_{ele}) of gyro-twystron is given by,

$$\eta_{ele}\,(\%) = (P_{out}/P_{dc})*100 \tag{2.10}$$

where $P_{dc}=V_b*I_b$. The beam voltage for gyrotron devices is in the order of 10 to 500 of kV, which is a measure of the kinetic parameter of particle. This is generally represented

in the form Lorentz factor (γ), which is given as $\gamma = 1 + (V_b / 511)$, where, the beam voltage in kV. The beam voltage detunes the cyclotron resonances, and this property is utilized in voltage tuning of gyrotron. Beam current *(I_b)* is calculated by,

$$I_b = \frac{P_{out} * 100}{V_b * \eta_{ele}} < I_{soc} \tag{2.11}$$

The beam voltage and current depend upon the space charge effect, which is measured by the voltage depression and limiting current. The space charge effect limits the performance of gyro-twystron and to reduce the space charge effects either the beam parameters or RF dimensions are altered. For minimizing the space charge effect limiting current I_l should be high and depressed voltage V_d should be low (In general $I_l \geq 2I_b$ and $V_d \leq V_b / 10$), and

$$I_l \approx 8500A\left[\gamma^* / \ln\left(\frac{r_w}{r_g}\right)\right] \tag{2.12}$$

where $\gamma^* = \gamma_0\left[1 - \left(1 - \beta_{zo}^2\right)^{\frac{1}{3}}\right]^{\frac{3}{2}}$

From the Figure 2.3, it can be seen that the limiting current of 790 A and depressed voltage 30 kV are obtained for the waveguide to guide centre radii ratio ~2.17 and the operating beam parameters *I_b and V_b* are well below the limiting current and depressed voltage.

The RF power can be increased with DC input power, which leads to efficiency degradation, and the efficiency of gyro-twystron is increased by operating device at high beam velocity pitch factor (α). Maximum available beam power for RF power conversion is proportional to $\alpha^2/(1+\alpha^2)$.

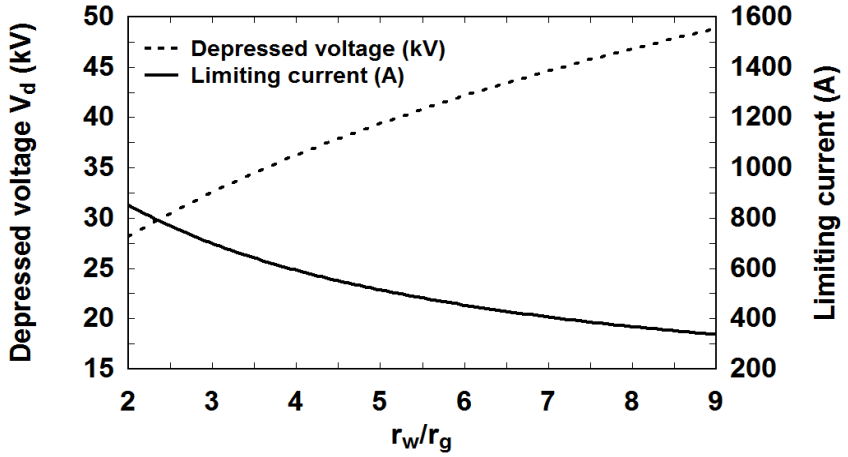

Figure 2.3 Limiting current and depressed voltage variation over the ratio of waveguide radius over the beam radius

However, the start current of gyro-twystron is directly proportional to the pitch factor (as mentioned in the waveguide design section). A careful increment in pitch factor is required to achieve the maximum efficiency with stability. The beam radius or guiding centre radius is positioned to couple the maximum kinetic energy of particles to the desired mode of RF wave. The guiding centre radius (r_g) is given by $r_g = \left(x_{m\pm s,i} r_w / x_{mn}\right)$ and the position of the annular electron beam is chosen far from the wall of the interaction structure to avoid the beam interception and especially in drift tubes, which are having smaller radii. The coupling coefficient is a measure of the interaction strength of electron beam with RF wave. Transverse electric field distributions in interaction structure as well as beam positions are varied to achieve the maximum coupling. The coupling coefficient C_{mn} is given by,

$$C_{mn} = \frac{\left[J_{m\pm s}\left(x_{mn}\, r_g / r_w\right)\right]^2}{x_{mn}{}^2 - m^2\ J_m^2\ x_{mn}} \tag{2.13}$$

From the Figure 2.4 and 2.5, it can be seen that fundamental azimuthal symmetric mode TE_{01} has strong coupling to electron beam near to $0.5*r_w$.

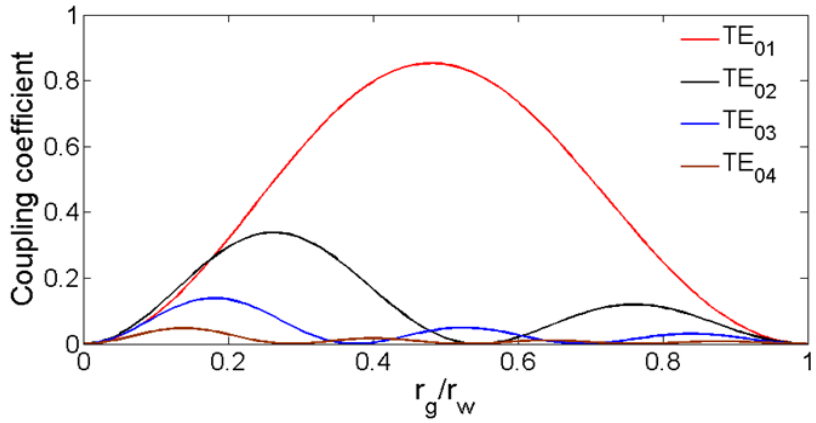

Figure 2.4. Coupling coefficient of TE modes over beam position.

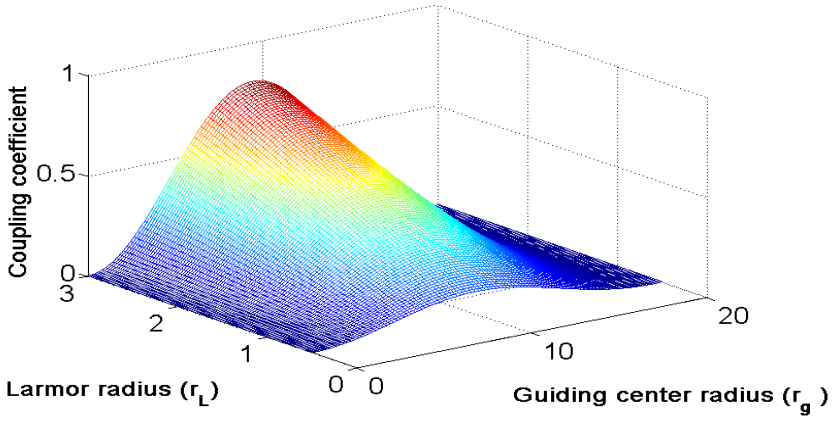

Figure 2.5 Coupling coefficient of TE_{01} mode over the guiding centre radius.

2.3 Multimode analysis of Gyro-twystron

Nonlinear analysis is employed to study the beam-wave interaction behaviour in the background of electromagnetic fields supported by the interaction structure. The present nonlinear theory is more general and it applies to all gyro-twystron amplifiers operating at an arbitrary cyclotron harmonics and any transverse electric mode. The beam-wave interaction mechanism primarily depends upon the synchronism between the cyclotron frequencies of gyrating electron beam, operating frequency of applied input signal. Maxwell's equation representing the field components of TE_{mn} mode excited in the circular waveguide is the starting point of our analysis. A source present term in the wave equation is included so that the effect of the electron beam can be included. Further, to obtain the wave equations in terms of the slow time scale variables, the transformation of

the coordinates from the cylindrical system to guiding centre system is required. This transformation can be incorporated by using Graf's summation theorem for Bessel's functions. Finally, the amplitude and phase of electromagnetic fields are governed by circuit equations. The electron beam dynamics, which govern the motion of the wave and electrons in the presence of a static axial magnetic field, (assuming the space charge fields to be negligible), which is explained with the help of relativistic Lorentz force equation for an electron interacting with a TE_{mn} fast waveguide mode.

In this theory, following assumptions are made; the space charge effects are ignored in interaction structure; all electrons have the same kinetic energy, i.e. mono-energetic at the entrance of interaction structure. A quasi-static system is assumed in the sense that all particles, entering the interaction region separated by integral multiples of the wave period, will travel along similar trajectories. With this assumption, the slow-time scale formalism can be followed, where the fast scale phenomena such as the electron cyclotron motion and the sinusoidal variations of the RF field are eliminated through averaging over a period while the more important slow-time scale spatial variations of the fields are retained.

The beam-wave interaction behaviour of gyro-twystron is studied by considering the interaction of the relativistic electron beam with the RF standing wave at the input cavity, which is excited by the input RF signal, and then considering the interaction of pre-bunched electron beam with one or more modes of travelling wave in the waveguide. The formalism of relativistic gyro-twystron is derived from the small signal linear theory of short input cavity and a large signal non-linear theory of output waveguide as follows:

2.3.1 Input Resonating Cavity

In the present analysis, a thin gyrating beam of electrons interacts with RF waves, which are represented by several transverse electric modes. The arrangement of the gyrating electron beam in a cylindrical cavity with all its coordinates is shown in Figure 2.6. Lorentz's force equation governing the particle dynamics in the presence of electric and magnetic fields is given by [86-87],

$$\frac{dp}{dt}+\frac{|e|}{\gamma m_e}p\times B_0=-|e|\left(E+\frac{1}{\gamma m_e}p\times B_0\right)\equiv a' \qquad \frac{dP}{dt}+\frac{|e|}{\gamma m_0}P\times B_0=$$

$$-|e|\left(E+\frac{1}{\gamma m_0}P\times B\right)\equiv a \quad (2.14)$$

where, B_0 is the applied magnetic field ($B_0 = B_0\hat{z}\; B_0 = B_0\hat{z}$), p is the momentum of the electron, γ is the relativistic mass factor defined as $\gamma=[1+p^2/(m_ec)^2]^{1/2}$, E and B are the RF electric magnetic fields, respectively.

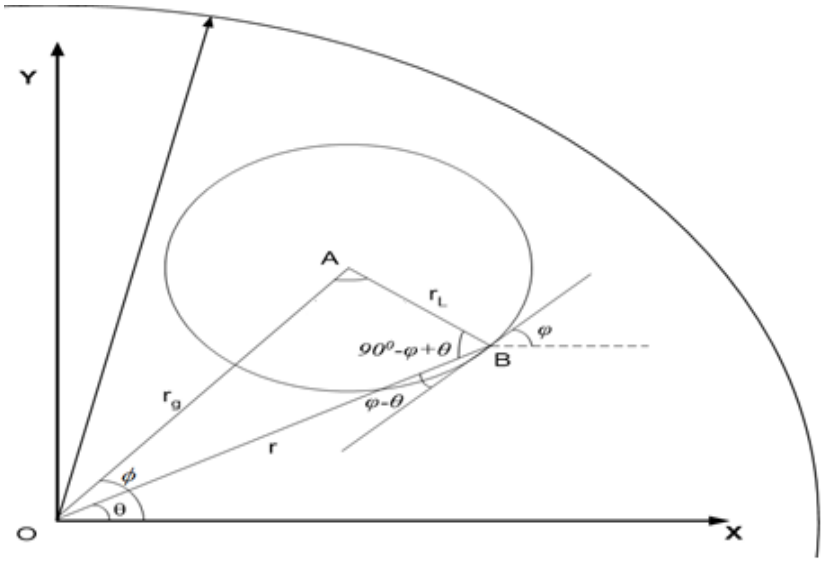

Figure 2.6 Arrangement of the gyrating electrons in Larmor orbit in the Cartesian as well as cylindrical coordinate systems.

Electrons' interaction with the applied RF signal in the input cavity results in perturbations in their momentum and phase, i.e., their momentum and phase deviate from the normal values they would have possessed, if there were no interaction. To facilitate

the tracking of changes in the momentum and phase of electrons and with an observation on the most suitable coordinate system, the cylindrical coordinate system in this context is considered. Therefore, the representing transverse momentum can be written as,

$$p_x + jp_y = jp_t \exp\left[j\left(\Omega\tau + \Phi_o\right)\right] \mathrm{p_x + ip_y = ip_t exp[i(\Omega\tau + \phi)]}$$

(2.15)

where, p_t $\mathrm{p_t}$and Φ_0 are the slow time scale magnitude and phase of transverse momentum. The term slow time scale indicates those temporal derivatives of the two, momentum and phase, are quiet less than operating frequency (ω) or the cyclotron frequency (Ω).

On simplifying equation (2.14), it can be expressed as,

$$a_x' + ja_y' = \frac{dp_x}{dt} + j\frac{dp_y}{dt} + \frac{\gamma_0}{\gamma}\Omega\left(p_y - jp_x\right) \tag{2.16}$$

and

$$a_x' - ja_y' = \frac{d\,p_x}{dt} - j\frac{d\,p_y}{dt} + \frac{\gamma_0}{\gamma}\Omega(p_y + jp_x) \tag{2.17}$$

By taking complex conjugates of equation (2.14) and, it can be obtained as,

$$\frac{d\,p_x}{dt} + j\frac{d\,p_y}{dt} = j\,p_t \exp[\,j(\Omega\tau + \Phi_o)](j\Omega + j\frac{d\phi}{dt}) + j\exp[\,j(\Omega\tau + \Phi_o)]\frac{d\,p_t}{dt}, \tag{2.18}$$

and

$$jp_x - p_y = -p_t \exp[\,j(\Omega\tau + \Phi_o)] \tag{2.19}$$

Substituting the above expressions into equations (2.17) and (2.18), it can be written as,

$$[a_x' + ja_y']\exp[-j(\Omega\tau + \Phi_o)] = -p_t(\Omega + \frac{d\Phi_o}{dt}) + j\frac{d\,p_t}{dt} + \frac{\gamma_0}{\gamma}\Omega p_t \tag{2.20}$$

and

$$[a_x' - ja_y']\exp[j(\Omega\tau + \Phi_o)] = -p_t(\Omega + \frac{d\Phi_o}{dt}) - j\frac{dp_t}{dt} + \frac{\gamma_0}{\gamma}\Omega p_t \tag{2.21}$$

Addition and subtraction of the above equations lead to the following:

$$\frac{dp_t}{dt} = \frac{j}{2}\{(a_x' - ja_y')\exp[j(\Omega\tau + \Phi_o)] - (a_x' + ja_y')\exp[-j(\Omega\tau + \Phi_o)]\} \tag{2.22}$$

$$\frac{d\Phi_o}{dt} = -\frac{1}{2}\{(a_x' - ja_y')\exp[j(\Omega\tau + \Phi_o)] + (a_x' + ja_y')\exp[-j(\Omega\tau + \Phi_o)]\} \times \frac{1}{p_t} - \Omega(1 - \frac{\gamma_0}{\gamma}) \tag{2.23}$$

and

$$\frac{dp_z}{dt} = a_z' \tag{2.24}$$

It is considered that the electron beam interacts with one or more competing modes in the cylindrical cavity. In terms of cylindrical coordinates, the total transverse electric and magnetic field component is given by [87],

$$E_t = \mathrm{Re}\left\{\sum_{q=1}^{N_q} A_q\{z,t\}e_q\{r,\theta\}e^{-j\omega_q t}\right\} \tag{2.25}$$

$$B_t = \mathrm{Re}\left\{\sum_{q=1}^{N_q} -\frac{j}{\omega_q}\frac{\partial}{\partial z}A_q\{z,t\}b_q\{r,\theta\}e^{-j\omega_q t}\right\} \tag{2.26}$$

where, $e_q\ (=\hat{z}\times\nabla_t\psi_q)\ \mathrm{e_n} = \hat{\mathrm{z}}\times\nabla_\mathrm{t}\Psi_\mathrm{n}$ and $b_q\ (=-\nabla_t\psi_q)\quad \mathrm{b_n} = -\nabla_\mathrm{t}\Psi_\mathrm{n}$ are the vector functions. Ψ_q is scalar or membrane function of q^{th} mode that satisfies the Helmholtz equation. The field amplitude $A_q\{z,t\} = A_{q_0}(\mathrm{t})\,f(z)$ and N_q is the number of modes that are assumed to be interacting.

$$\psi_q\{r,\theta\} = C_{m_q n_q} J_{m_n}\left\{k_{m_q n_q} r\right\} \exp[jm_q\theta] \tag{2.27}$$

and

$$C_{m_q n_q} = \frac{1}{\sqrt{[\pi(x^2_{m_q n_q} - m_q^2)]} \times J_{m_q}\left\{x_{m_q n_q}\right\}} \tag{2.28}$$

$C_{m_n l_n} = \left\{\sqrt{\left[\pi\left(x^2_{m_n l_n} - m^2\right)\right]} * J_{m_n}\left(x_{m_n l_n}\right)\right\}^{-1}$

After defining the RF fields, the components a'_x a'_y a'_z can be determined subsequently. As the cylindrical coordinate system is intended to use, the two transverse components a'_x, and a'_y a_x can be defined a_y in terms of a'_r and a_θ as:

$$a'_x = a'_r\cos\theta - a'_\theta\sin\theta, \text{ and } a'_y = a'_r\cos\theta + a'_\theta\sin\theta \tag{2.29}$$

To determine the components a'_r a_θ and a'_z, the momentum vector p in the equation (2.14) defined in a cylindrical coordinate system as,

$$p = p_t\cos(\Phi-\theta)\hat{r} + p_t\sin(\Phi-\theta)\hat{\theta} + p_z\hat{z} \tag{2.30}$$

where, $\Phi = \Omega\tau + \Phi_o$.

Now, $B_t = \mathrm{Re}\left\{\sum_{q=1}^{N_q}\frac{j}{\omega_q}\frac{\partial}{\partial z}A_q\{z,t\}\nabla_t\psi_q e^{-j\omega_q t}\right\}$ and $E_t = \mathrm{Re}\left\{\sum_{q=1}^{N_q}A_q\{z,t\}\hat{z}\times\nabla_t\psi_q e^{-j\omega_q t}\right\}$

(2.31)

Since, $b_q = -\nabla_t\psi_q = -\frac{\partial\psi}{\partial r}\hat{r} - \frac{1}{r}\frac{\partial\psi}{\partial\theta}\hat{\theta}$, and $e_q = \hat{z}\times\nabla_t\psi_q = -\frac{1}{r}\frac{\partial\psi}{\partial\theta}\hat{r} + \frac{\partial\psi}{\partial r}\hat{\theta}$,

therefore, the components of magnetic and electric fields can be obtained as:

$$B_r = \mathrm{Re}\left\{\sum_{q=1}^{N_q}C_{m_q n_q}\frac{j}{\omega_q}\frac{\partial}{\partial z}A_q\{z,t\}k_{m_q n_q}J'_{m_q}\left\{k_{m_q n_q}r\right\}\exp[j(m_q\theta-\omega_q t)]\right\} \tag{2.32}$$

$$B_\theta = \mathrm{Re}\left\{\sum_{q=1}^{N_q} C_{m_q n_q} \frac{-1}{\omega_q}\frac{\partial}{\partial z} A_q\{z,t\}\frac{m_q}{r} J_{m_q}\left\{k_{m_q n_q} r\right\}\exp[j(m_q\theta-\omega_q t)]\right\} \tag{2.33}$$

$$B_z = \mathrm{Re}\left\{\sum_{q=1}^{N_q} C_{m_q n_q} \frac{j}{\omega_q} A_q\{z,t\} k_t^2 J_{m_q}\left\{k_{m_q n_q} r\right\}\exp[j(m_q\theta-\omega_0 t)]\right\} \tag{2.34}$$

$$E_r = \mathrm{Re}\left\{\sum_{q=1}^{N_q} -C_{m_q n_q} \frac{jm_q}{r} A_q\{z,t\} J_{m_q}\left\{k_{m_q n_q} r\right\}\exp[j(m_q\theta-\omega_q t)]\right\} \tag{2.35}$$

and

$$E_\theta = \mathrm{Re}\left\{\sum_{q=1}^{N_q} C_{m_q n_q} k_{m_q n_q} A_q\{z,t\} J'_{m_q}\left\{k_{m_q n_q} r\right\}\exp[j(m_q\theta-\omega_q t)]\right\} \tag{2.36}$$

Now, on evaluating,

$$\begin{aligned} p\times B = {} & [p_t \sin(\Phi-\theta)B_z - p_z B_\theta]\hat{r} - [p_t\cos(\Phi-\theta)B_z - p_z B_r]\hat{\theta} + \\ & \hat{z}[p_t\cos(\Phi-\theta)B_\theta - p_t\sin(\Phi-\theta)B_r] \end{aligned} \tag{2.37}$$

Therefore,

$$a'_r = -|e|(E_r + v_t\sin(\Phi-\theta) - v_z B_\theta$$

$$a'_\theta = -|e|(E_\theta - v_t\cos(\Phi-\theta) + v_z B_r)$$

$$a'_z = -|e|(v_t\cos(\Phi-\theta)B_\theta - v_z\sin(\Phi-\theta)B_r)$$

$$a'_x = a'_r\cos\theta - a'_\theta\sin\theta, \text{ and } a'_y = a'_r\cos\theta + a'_\theta\sin\theta \tag{2.38}$$

Taking simplest expression, a'_z, from the above, the following expression can be obtained after algebraic simplification as:

$$a_z' = -|e| v_t \,\mathrm{Re}\left\{\sum_{q=1}^{N_q} \frac{C_{m_q n_q} k_{m_q l_q}}{\omega_q} \frac{\partial}{\partial z} A_q\{z,t\}[J_{m_q-1}\{k_{m_q n_q} r\}\exp[j(m_q-1)\theta - \omega_q t + j\Phi] + J_{m_q+1}(k_{m_q n_q} r)\exp[j(m_q+1)\theta - \omega_q t - j\Phi]\right\} \tag{2.39}$$

Considering the finiteness of Larmor radius of the beamlet, the RF wave-electron interaction from the co-ordinate system centered at the centre of beamlets considered, rather than coordinate system centred along axis of the cavity. This coordinate transformation can be performed using Graf's addition theorem [88-89], and it can be expressed in the following form:

$$J_v\{\eta R_{il}\} e^{jv(\theta i - \vartheta_{il})} = \sum_{\mu=-\infty}^{\infty} J_{v+\mu}\{\eta R_{il}\} J_\mu\{\eta r_l\} e^{[i\mu(\pi - \theta_l + \vartheta_{il})]}, i \neq l \tag{2.40}$$

where, $(r_v, \theta_v)(\mathrm{r_j}, \theta_\mathrm{j})$ and $(r_l, \theta_l)(\mathrm{r_j}, \theta_\mathrm{j})$ are polar coordinates centred at two different positions with global coordinates O_j, O_l. $(R_{il}, \vartheta_{il})(\mathrm{R_{jl}}, \vartheta_{\mathrm{jl}})$ are the polar coordinates of O_l $\mathrm{O_l}$ with respect to O_i. This expression is valid only provided that $r_l < R_{il}$ $\mathrm{r_1 < R_{jl}}$. The right-hand side of the equation (2.39) $\mathrm{a_z}$ can be written in a suitable form to apply the Graf's theorem as:

$$a_z' = |e| v_t \,\mathrm{Re}\left\{\sum_{q=1}^{N_q} \frac{C_{m_q n_q}}{\omega_q} \frac{\partial}{\partial z} A_q\{z,t\} e^{-j\omega_q t}[e^{i(m_q-1)\theta_0 + j\Phi} J_{m_q-1}\{k_{m_q n_q} r\} \exp[j(m_q-1)(\theta-\theta_0)] + J_{m_q+1}\{k_{m_q n_q} r\}\exp[j(m_q+1)\theta - \omega_q t - j\Phi]\right\} \tag{2.41}$$

After transformation to the new co-ordinate system using an aforementioned theorem, the following changes occur in the above equation:

$$\sum_{\mu=-\infty}^{\infty} J_{m_q-\mu}\{k_{m_q n_q} r_g\} J_{-\mu+1}\{k_{m_q n_q} r_L\} e^{-j(\mu-1)(\pi/2-\Phi+\theta_0)},$$

and,

$$\frac{dp_x}{dt} + j\frac{dp_y}{dt} = jp_t \exp[j(\Omega\tau + \Phi_o)](j\Omega + j\frac{d\Phi_0}{dt}) + j\exp[j(\Omega\tau + \Phi_0)]\frac{dp_t}{dt}$$

From the abovementioned equations, by considering $\mu = s\mu = s$, for which $s\Omega \approx \omega$ where, s is the harmonic number and replacing Φ by $\Omega\tau + \Phi_0\ \Omega\tau + \phi$, it can be written as [86], [90],

$$\frac{dp_z}{dt} = a_z' = |e| v_t \,\mathrm{Re}\left\{\sum_{n=1}^{N_q} \frac{C_{m_q n_q}}{\omega_q}\frac{\partial}{\partial z}A_q\{z,t\}[J_{m_q - s_q}\left\{k_{m_q n_q} r_g\right\}\frac{\partial J_S\left\{k_{m_q n_q} r_L\right\}}{\partial r_L}e^{-j\Lambda_q}]\right\} \quad (2.42)$$

where, $\Lambda_q = (\omega_q - s\Omega)\tau + \omega_q t_0 - s_q\Phi_0 - (m_q - s_q)\phi$

$$\Lambda = (\omega_0\text{-}s\Omega)\tau + \omega_0 t_0\text{-}s\phi\text{-}(m_n\text{-}s)\theta_0$$

$$\frac{dp_t}{dt} = -|e|\,\mathrm{Re}\left\{\sum_{q=1}^{N_q}\frac{C_{m_q n_q}}{\omega_q}\left[\omega_q A_q\{z,t\} + jv_z\frac{\partial}{\partial z}A_q\{z,t\}\right]\times\left[\begin{array}{l} J_{m_n - s_q}\left\{k_{m_q n_q} r_g\right\} \\ \dfrac{\partial J_S\left\{k_{m_q n_q} r_L\right\}}{\partial r_L}e^{-j\Lambda_q}\end{array}\right]\right\} \quad (2.43)$$

$$\frac{d\Lambda}{dt} = \frac{s|e|}{p_t}\mathrm{Re}\left\{\sum_{n=1}^{N}\frac{Cm_q n_q}{\omega_q}j[\omega_q A_q\{z,t\} + jv_z\frac{\partial}{\partial z}A_q\{z,t\} - \frac{k_{m_q n_q}^2}{s\Omega\gamma_0}A_q\{z,t\}]\right.$$
$$\left.\times[J_{m_q - s_q}\left\{k_{m_q n_q} r_g\right\}\frac{s\partial J_{s_q}\left\{k_{m_q n_q} r_L\right\}}{\partial r_L}e^{-j\Lambda_q}]\right\} + \Omega\left(\frac{\omega_q}{\Omega} - s_q\frac{\gamma_0}{\gamma}\right) \quad (2.44)$$

By using the energy equation and inequalities proposed by Bratman *et al.*, a spatial derivative of phase and energy of transverse electric mode is obtained. The axial length (z) is normalized by $Z=\omega z/c$, and a slow varying momentum phase is introduced *($\theta=\Lambda$-$k_z z$)* [86-87],

$$\frac{du}{dZ}=|e|\left\{\sum_{q=1}^{N_q}\frac{ep_t}{\gamma_0 mcp_z}\frac{C_{m_q n_q}}{\omega_q}J_{m_n-s_q}\left\{k_{m_q n_q}r_g\right\}\frac{\partial J_s\left\{k_{m_q n_q}r_L\right\}}{\partial r_L}\mathrm{Re}\left[A_{q_0}e^{-j\theta}\right]\right\} \tag{2.45}$$

$$\frac{d\theta}{dZ}=|e|\gamma_0 mc\left\{\sum_{q=1}^{N_q}\frac{\left(\delta_0-w\left(1-\beta_{ph}^{-2}\right)\right)}{p_t}+\frac{1}{p_z p_t}\frac{C_{m_q n_q}}{\omega_q}J_{m_n-s_q}\left\{k_{m_q n_q}r_g\right\}\frac{\partial J_s\left\{k_{m_q n_q}r_L\right\}}{\partial r_L}}{\left[1-w\left(1-\beta_{ph}^{-2}\right)-\left(\frac{p_t}{\gamma_0 mc}\right)^2\left(1-\beta_{ph}^{-2}\right)/(1-\beta_{z0}/\beta_{ph})\right]\mathrm{Re}\left[iA_{q_0}e^{-j\theta}\right]}\right\} \tag{2.46}$$

As compared to the guiding centre radius, smaller Larmor radius is assumed, which follows,

$$J_{s_q-1}\left(k_{m_q n_q}\right)\approx\frac{s^{s-1}\left(1-\beta_{ph}^{-2}\right)^{s_q-1/2}\beta_{t_0}^{s-1}\left(\sqrt{1-w}\right)^{s-1}}{2^{s-1}(s-1)!(1-\beta_{z0}/\beta_{ph})^{s-1}},\ \text{where}\ w=\frac{2}{\beta_{to}^2}\left(1-\beta_{z_0}/\beta_{ph}\right)u$$

With the further simplification, the single-mode formalism [61] is extended in the multimode theory of gyro-twystron, and the spatial variation of normalized energy (w) and phase (θ) are deduced as following,

$$\frac{dw}{d\zeta}=\sum_{q=1}^{N_q=1}\left(\frac{p_t^{s_q}}{p_z}\right)\mathrm{Re}\left(F_{cq}f(\zeta)e^{-j\theta_q}\right) \tag{2.47}$$

$$\frac{d\theta}{d\zeta}=-\sum_{q=1}^{N_q=1}\frac{w-s_q\Omega/\omega_q}{p_z}+\frac{s_q w p_t^{s_q-2}}{p_z}\mathrm{Re}\left(jF_{cq}f(\zeta)e^{-j\theta_q}\right)\left(f(\zeta)-j\frac{p_z}{w}\frac{df(\zeta)}{d\zeta}\right) \tag{2.48}$$

where, s_q is the harmonic number of q^{th} mode, p_z is the axial momentum, p_t is the orbital momentum of the electron, phase θ_q, Ω is the non-relativistic cyclotron frequency, the

normalized length $\zeta = \frac{\beta_{t_0}^2}{2\beta_{zo}} \frac{\left(1-\beta_{ph}^{-2}\right)}{(1-\beta_{zo}/\beta_{ph})} Z$. The normalized RF field amplitude, F_{cq} of q^{th} mode at the input cavity is given as,

$$F_{cq} = \sum_{q=1}^{N_q} \frac{eA_{0q}}{m_0 c\omega_q} \frac{\left(k_{tq}/k_q\right)^{s-2}}{(\Omega/\omega_q)^{s_q-1}\left(s_q-1\right)!2^{s_q+1}} C_{1q} \tag{2.49}$$

and the complex gain function Φ_q is defined as,

$$\Phi_q = \frac{1}{F_{cq}} \int_0^{L_c} \left(\frac{1}{2\pi} \int_0^{2\pi} \frac{p_t^{s_q}}{p_z} e^{j\theta} d\theta \right) f(\zeta) d\zeta \tag{2.50}$$

where, $C_{1q} = \left\{ J_{m_q \pm s_q}(k_{tq} r_g) \right\} / \left\{ (x_{m_q p_q}^2 - m_q^2) J_{m_q}^2 (x_{m_n p_q}^2) \right\}$, $x_{m_q p_q}$ is the Eigen value of q^{th} TE_{mn} mode, m_q is an azimuthal index of q^{th}mode, k is the wave number, k_t is the transverse wave number, r_g is the electron guiding centre radius, '$\pm$' sign in Bessel's function represent co- and counter rotation, respectively. The amplitude of RF input signal is expressed as $A_{0q} = \sqrt{4 I_{0q} P_{in} Q_q / P_{0t} Q_{cpl_q}}$, where, P_{in} is the RF input power, Q is the total quality factor, Q_{cpl} is the coupling quality factor, $P_{0t} = \left(\beta_{t0}^2 / 2\left(1-w_0^{-1}\right)\right) V_b I_b$ is the beam power of gyrating particle at the input end, and the normalized beam current parameter of q^{th} mode I_{0q} is defined as,

$$I_{0q} = \frac{eI_b}{w_0 m_0 c^3} \left(\frac{1}{\left(s_q-1\right)!2^{s_q}} \right)^2 \left(\frac{k_{tq}/k_q}{\Omega/\omega_q} \right)^{2\left(s_q-1\right)} \left(\frac{1}{\int_0^{L_c} f(\zeta)^2 df} \right) C_{1q} \tag{2.51}$$

where, L_c is the length of the cavity and I_b is the DC beam current. The complex gain function (C_Φ) in equation (2.50) is linearized with respect to small RF electric field developed at the short input cavity as,

$$C_{\Phi} \approx 4\frac{\gamma_0^3}{P_{t0}^{2(3-s_q)}}\mu^2\frac{1}{\left(\Theta^2-\pi^2\right)}\left[\begin{array}{l} js_q\Theta\left(\Theta^2-\pi^2\right)-2s_q\pi^2\left(1+e^{-j\Theta}\right)+\mu \\ \times\left(-j\left(\Theta^2+\pi^2\right)+\dfrac{8\pi^2}{\left(\Theta^2-\pi^2\right)}\Theta\left(1+e^{-j\Theta}\right)+j2\pi^2e^{-j\Theta}\right)\end{array}\right]$$

(2.52)

This also depends on the electron transit angle at the end of the input cavity and the parameter $\mu=\left(p_{t0}^2/2p_{z0}\gamma_0\right)L_c$, which is responsible for the disturbance in cyclotron resonance frequency with the change in electron energy.

2.3.2 Field-Free Drift Region

Before electrons enter the drift tube, their energy, momentum and phase are perturbed in the short input cavity by the RF field [61]. Electron phase at the output of the drift tube is given as,

$$\theta_{dr_q}=\theta_1-\int_{L_c}^{L_{dr}}\left\{\left(w_1-\Omega/\omega_q\right)/p_{z0}\right\}d\zeta \tag{2.53}$$

where, w_1, p_{z1}, and θ_1 are the normalised energy variable, momentum and electron phase at the input end of the drift tube, respectively, and L_c and L_{dr} are the length of the cavity and the drift tube, respectively. Since the field at the input cavity is small, we can linearise the equation (2.53) over the length as,

$$\theta_{dr_q}=\bar{\theta}_0-\Theta_{dr}-\mathrm{X}_q\cos\bar{\theta}_0 \tag{2.54}$$

where, the transit angle of unperturbed electron Θ_{dr} at the drift tube end and the bunching parameter 'X' are written as

$$\Theta_{dr}=\int_0^{L_c+L_{dr}}\left\{\left(w_0-\Omega/\omega_q\right)/p_{t0}\right\}d\zeta \tag{2.55}$$

$$X_q = 4\left\{ p_{t0}^{s_q} / p_{z0}^2 \right\}\left\{ F_{cq} / L_c \right\}\left\{ \left(L_c^2 - \Theta_{dr}^2 \right) / \left(\Theta_{dr}^2 - \pi^2 \right) \right\} \pi \cos\left(\Theta_{dr} / 2 \right) \tag{2.56}$$

2.3.3 Output Waveguide Section

Bunched electrons with finite bunching factor enter the output waveguide, where they interact with the RF field excited by the pre-bunched electron beam. The interaction between several TE modes and the electron beam at the output section of gyro-twystron is studied through a steady-state multi-mode, multi-harmonic code. In the present case, the following initial and boundary conditions [78] are applied,

$$w(0) = 1;\ \theta(0) = \theta_w - X_q \cos\theta_w - \Theta_{dr}\ ;\ F_q\left(z = 0 \right) = 0$$

where, $\theta_w \in [0, 2\pi]$. The RF field equation of l^{th} TE mode in the circular waveguide[91] is written as,

$$H_{zl} = \mathrm{Re}\left(F_l\left(z \right) \psi_l e^{-j\omega_l t} \right) \tag{2.57}$$

The total magnetic field for 'l' number of modes is accounted through the principle of superposition as,

$$H_z = \sum_l H_{zl} = \sum_l \mathrm{Re}\left(F_l\left(z \right) \psi_l e^{-j\omega_l t} \right) \tag{2.58}$$

where, $\psi_l = J_{m_l}\left(k_{\perp l} r \right) e^{m_l \theta}$, $F_l\left(z \right)$ is the field along the axial length and ω_l is the angular frequency of the l^{th} TE mode,

$$\sum_l \left(\nabla^2 H_{zl} + k_l^2 H_{zl} \right) = -\left(\nabla \times \vec{J} \right)_z \tag{2.59}$$

For the axial propagating wave, equation (2.59) is deduced as,

$$\sum_l \mathrm{Re}\left\{ \left(\frac{d^2}{dz^2} + k_{zl}^2 \right) F_l\left(z \right) \psi_l e^{-i\omega_l t} \right\} = -(\nabla \times \vec{\mathrm{J}})_z \tag{2.60}$$

Multiplying both the side of equation (2.60) by $\psi_q^* e^{j\omega_q t}$ and $\int_0^{\frac{2\pi}{\omega_q}}\int_0^{r_w}\int_0^{2\pi} d\phi r dr dt$, hence the left-hand side becomes,

$$\int_0^{\frac{2\pi}{\omega_q}}\int_0^{r_w}\int_0^{2\pi}\sum_l \left\{\begin{matrix}\left(\frac{d^2}{dz^2}+k_{zl}^2\right)\\ F_l(z)\psi_l\,\psi_q^* e^{j(\omega_q-\omega_l)t}\end{matrix}\right\}+\left\{\begin{matrix}\left(\frac{d^2}{dz^2}+k_{zl}^2\right)\\ F_l^*(z)\psi_l^*\,\psi_q^* e^{j(-\omega_l-\omega_q)t}\end{matrix}\right\} d\phi r dr dt \qquad (2.61)$$

The orthogonality law $\begin{cases}\int_0^{2\pi}\int_0^{r_w}\left(\psi_l\psi_q^k\right) r dr d\phi = \delta_{lq}\pi r_w^2 C_q\\ \int_0^{2\pi}\int_0^{r_w}\left(\psi_l^*\psi_q^k\right) r dr d\phi = 0 \quad (l\neq q)\end{cases}$

where, $C_q = \left\{x_{m_q n_q}^2 - m_q^2\right\} * \left\{J_{m_q}^2\left(x_{m_q n_q}^2\right)/x_{m_q n_q}^2\right\}$. Using the orthogonally law, equation (2.61) deduced to,

$$\left(\frac{d^2}{d\zeta^2}+k_{zq}^2\right)F_q(\zeta) = -\frac{\omega_q}{\pi^2 r_w^2 C_q}\int_0^{\frac{2\pi}{\omega_q}}\int_0^{r_w}\int_0^{2\pi}\left\langle(\nabla\times J)_z\,\psi_q^*\right\rangle e^{-j\omega_q t} d\vartheta r dr dt \qquad (2.62)$$

where,

$$\psi_q^* = J_{s_q}'\left(k_{tq}r_L\right)J_{m_q-s_q}\left(k_{tq}r_g\right)\times e^{j\left(s_q\theta+\left(m_q-s_q\right)\phi\right)}$$

and

$$\vec{J} = \frac{2\pi I_b}{\omega_q r}\sum_{i=1}^{Ne} W_i\,\delta(r-r_i)\,\delta(\theta-\theta_i)\,\delta(t-t_i)\frac{\beta_{ti}}{\beta_{zi}}$$

Solving the right-hand side of equation (2.62), we get the field equation as,

$$\left(\frac{d^2}{d\zeta^2}+k_{zq}^2\right)F_q(\zeta) = \frac{2I_b k_{tq} e}{\pi r_w^2 C_q}\left(\sum_{i=1}^{N} W_i\frac{\beta_{ti}}{\beta_{zi}}J_{s_q}'\left(k_{tq}r_L\right)J_{m_q-s_q}\left(k_{tq}r_g\right)e^{-j\left(s_q\theta+\left(m_q-s_q\right)\phi-\omega_q t\right)}\right) \qquad (2.63)$$

where, W_i is the weighting factor, which is defined as $\sum_i^{Ne} W_i = 1$, and N_e represents the total number of electrons. The electron dynamic's dependency on Gaussian distribution is employed for accounting the axial velocity spread as $g(p_{t,}\,p_z) = A_n\delta(\gamma-\gamma_0)e^{-\left[(p_z-\bar{p}_z)^2/2\Delta p_z{}^2\right]}$, where, $\bar{p}_z$ is the mean value of axial momentum

and Δp_z is the standard deviation from the axial momentum and A_n is the normalization constant. For i^{th} particle, the weighting factor in the form Gaussian distribution model is given as $W_i = A_n e^{-\left[(p_{zi}-\bar{p}_z)^2/2\Delta p_z{}^2\right]}$. The motion of an electron in the RF interaction circuit is governed by[91],

$$d\vec{p}/dt = -e\vec{v}\times\left(B_0\hat{\zeta}\right) - e(\vec{\mathrm{E}}+\vec{v}\times\vec{B}) + \mathrm{e}\left(\vec{v}\times\left(dB_0/2d\zeta\right)\hat{r}\right) \tag{2.64}$$

where, $\vec{p}$ is momentum, $\vec{E}$ and $\vec{B}$ are the electric and magnetic fields of the RF wave, respectively, v is the velocity of the particle, B_0 is applied DC magnetic field and $\left(1/2B_0\right)\left(dB_0/d\zeta\right)$ is the measure of magnetic field tapering. The following set of equations representing the axial variation of transverse momentum, axial momentum, phase, guiding centre radius and guiding centre angle respectively, describe the electron motion in the RF interaction region in the presence of field as,

$$\frac{dp_t}{d\zeta} = m_e c\frac{1}{2B_0}\frac{dB_0}{d\zeta}\beta_t - \frac{ec\mu_0}{\beta_z}\mathrm{Re}\left\{\sum_q\left(\begin{array}{l}\dfrac{1}{k_{tq}}\left(j\omega_{qF}F_q(\zeta)+v_z F_q^{'}(\zeta)\right)J_{s_q}^{'}\left(k_{tq}r_L\right)\\ \times J_{m_q-s_q}\left(k_{tq}r_g\right)\times e^{-j\left(s_q\theta+\left(m_q-s_q\right)\phi-\omega_q t\right)}\end{array}\right)\right\} \tag{2.65}$$

$$\frac{dp_z}{d\zeta} = m_e c\frac{1}{2B_0}\frac{dB_0}{d\zeta}\frac{\beta_t^2}{\beta_z} - \frac{e\mu_0\beta_t}{\beta_z}\mathrm{Re}\left\{\sum_q\left(\begin{array}{l}\dfrac{1}{k_{tq}}F_q^{'}(\zeta)J_{s_q}^{'}\left(k_{tq}r_L\right)\\ J_{m_q-s_q}\left(k_{tq}r_g\right)e^{-j\left(s_q\theta+\left(m_q-s_q\right)\phi-\omega_q t\right)}\end{array}\right)\right\} \tag{2.66}$$

$$\frac{d\theta}{d\zeta} = \frac{eB_0}{p_z} - \frac{\mu_0 e}{\gamma c\beta_z\beta_t}\mathrm{Re}\left\{\sum_q\left(\begin{array}{l}\dfrac{1}{k_{tq}^2}\left(\dfrac{s_q\omega_q}{r_L}F_q(\zeta) - k_{tq}^2\beta_t cF_q(\zeta) - \dfrac{js_q c}{r_L}\beta_z F_q^{'}(\zeta)\right)\\ \times J_{s_q}\left(k_{tq}r_L\right)J_{m_q-s_q}\left(k_{tq}r_b\right)e^{-j\left(s_q\theta+\left(m_q-s_q\right)\phi-\omega_q t\right)}\end{array}\right)\right\} \tag{2.67}$$

$$\frac{dr_g}{d\zeta} = -\frac{1}{2B_0}\frac{dB_0}{d\zeta} r_g + \frac{\mu_0}{c\beta_z B_0}\sum_q \left\{ \begin{aligned} &\frac{1}{k_{tq}} J_{s_q}\left(k_{tq} r_L\right) J'_{m_q - s_q}\left(k_{tq} r_g\right).\mathrm{Re}\left[\begin{aligned} &\left(c\beta_z F_q'(\zeta) + j\omega_q F_q(\zeta)\right) \\ &e^{-j\left(s_q\theta + \left(m_q - s_q\right)\phi - \omega_q t\right)} \end{aligned} \right] \\ &\times - \left[\begin{aligned} &J_{s_q - 1}\left(k_{tq} r_L\right) J_{m_q - s_q - 1}\left(k_{tq} r_g\right) \\ &\times - J_{s_q + 1}\left(k_{tq} r_L\right) J_{m_q - s_q + 1}\left(k_{tq} r_g\right) \end{aligned} \right] \mathrm{Im}\left[\begin{aligned} &\frac{1}{2} c\beta_t F_q(\zeta) \\ &e^{-j\left(s_q\theta + \left(m_q - s_q\right)\phi - \omega_q t\right)} \end{aligned} \right] \end{aligned} \right\} \quad (2.68)$$

$$\frac{d\phi}{d\zeta} = \frac{\mu_0 c}{r_g B_0 \beta_z}\sum_q \left\{ \begin{aligned} &\frac{1}{k_{tq}^2}\frac{m_q - s_q}{r_g} J_{s_q}\left(k_{tq} r_L\right) J_{m_q - s_q}\left(k_{tq} r_g\right) \mathrm{Im}\left[\begin{aligned} &\left(c\beta_z F_q'(\zeta) + j\omega_q F_q(\zeta)\right) \\ &e^{-j\left(s_q\theta + \left(m_q - s_q\right)\phi - \omega_q t\right)} \end{aligned} \right] - \\ &\times \left[\begin{aligned} &J_{s_q - 1}\left(k_{tq} r_L\right) J_{m_q - s_q - 1}\left(k_{tq} r_g\right) + \\ &J_{s_q + 1}\left(k_{tq} r_L\right) J_{m_q - s_q + 1}\left(k_{tq} r_g\right) \end{aligned} \right] \mathrm{Re}\left[\frac{1}{2} c\beta_t F_q(\zeta) e^{-j\left(s_q\theta + \left(m_q - s_q\right)\phi - \omega_q t\right)} \right] \end{aligned} \right\} \quad (2.69)$$

$$dt / d\zeta = 1 / c\beta_z \quad (2.70)$$

where, β_t is the normalized transverse velocity, β_z is the normalized axial velocity, μ_0 is the permeability, the subscript q represents the number of modes. The total electronic efficiency is given by,

$$\eta_{ele} = \frac{\gamma_0 - \left\langle \gamma \;\; \zeta = L_{out} \right\rangle_{\theta,\phi}}{\gamma_0 - 1} = \frac{{\beta_{t_o}}^2}{2(1 - k_z \beta_{z_0} / k)(1 - \gamma_0^{-1})} . \eta_\perp \quad (2.71)$$

Table 2.1 Design parameters of gyro-twystron [57]

Particulars	**Values**
Beam Voltage	440 kV
Beam Current	230 A
Pitch factor	1.05
Velocity Spread	7 %
Pre-drift section length	32 mm
Input cavity radius	28.1 mm
Input cavity length	17.3 mm
Drift section radius	15 mm
Drift section length	143.6 mm
Waveguide radius	19.5 mm
Waveguide length	250 mm
Guiding centre radius	0.46 r_w

2.4 Numerical Benchmarking

In the present work, a self-consistent, nonlinear, multimode code supports harmonics has been developed for studying the transient behaviour of an X-band gyro-twystron. The solution for electron motion and the field developed by the electrons are obtained by solving a set of self-consistent coupled equations, which are given in Section 2.3. In self-consistent calculations, the equation of motion for the electron and electromagnetic field are solved simultaneously; effect of electron kinematics and field equations on each other, considered and updated iteratively. Figure 2.7 shows the axial growth of the RF power in the desired TE_{01} mode and other adjacent parasites, including TE_{11}, TE_{21}^{2} and TE_{02}^{2} modes. The saturated RF output power in the operating mode was observed as ~19.6 MW with a power conversion efficiency of ~19.4 % at 10 GHz. Other unwanted parasites, including TE_{11}, TE_{21}^{2} are well suppressed except TE_{02}^{2} mode that shares ~1 MW of power. The variation of energy and phase of gyrating electrons are shown in Figures 2.8(a) and 2.8(b), respectively. In gyro-twystron, electrons gaining energy from the RF field should be less than the energy lost to the RF field. Figure 2.8 (a) shows the normalized energy which evidence that some gyrating electrons have higher energy than their initial energy and the rest of electrons have lower, because some electrons lost energy to the RF field, while others gained energy from the field. The variation of phase due to the Doppler shift along the axial position of the RF circuit for 7% of spread is shown in Figure 2.8 (b). Figure 2.9 is the direct comparison of the present studies with the earlier experimental results. However, the passing agreement between the present analytical due to the following reason:

The peak power and the efficiency were limited by the parasites and the degree of suppression of these modes is studied through the nonlinear, self-consistent, multimode

code supports harmonics. To simplify the analysis, the following assumptions were made including the absence of space charges, no drift in guiding centre radius, magnetic field and in wall radius. Besides, at unity pitch factor and at the current higher than 200 A the RF output power in the operating mode dominates over the parasites that lead to a significant error. However, there is no big metric difference in the RF output power, and the present nonlinear analysis predicts ~19.6 MW. These results are found to be in close agreement with the experimentally reported ~21 MW at the University of Maryland, USA by Latham *et al.*

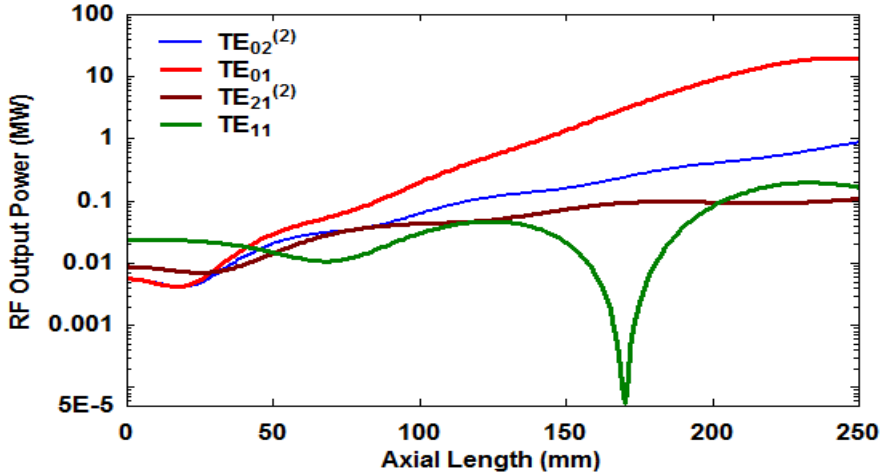

Figure 2.7 Growth of RF output power in desired mode as well as competing mode along the axial position of waveguide

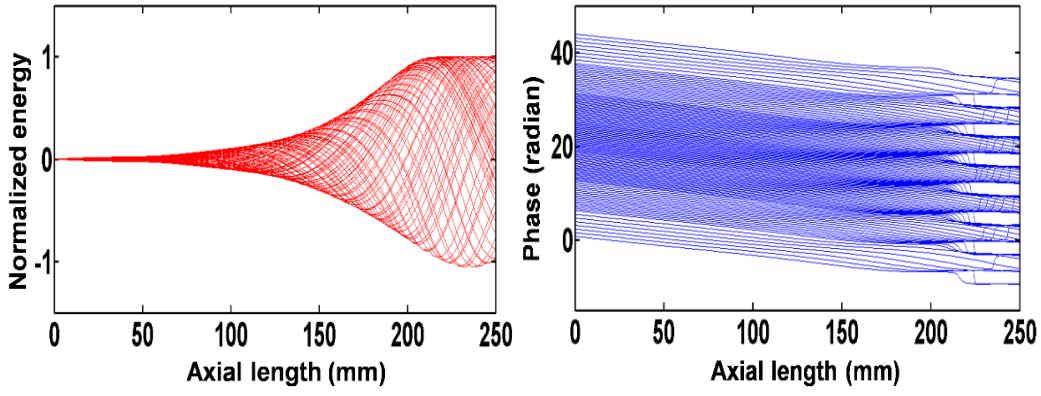

(a) (b)

Figure 2.8 Normalized energy and electron along the axial position of waveguide (b) phase of the electron along the axial position of waveguide

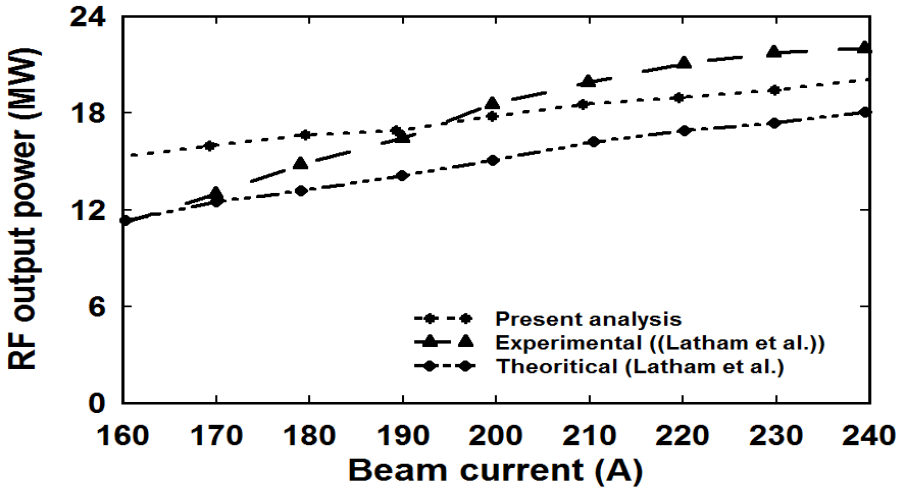

Figure 2.9. Comparison of RF power variation over the beam current

2.5 Conclusion

In the present chapter, the design methodology of the gyro-twystron amplifier has been developed along with the beam wave interaction theory. The design issues of each component of a gyro-twystron amplifier such as the cavity, drift tube, and waveguide are discussed, independently. The full RF wave-electron beam interaction behaviour of a gyro-twystron has been studied using a steady state nonlinear self-consistent code includes multiple modes at multiple harmonics. The present nonlinear transient behaviour of Gyro-twystron has been benchmarked with an experimentally tested gyro-twystron in X-band by Latham *et al.* at the University of Maryland as follows: Latham *et al.* (experiment) Vs present nonlinear results agreed by 6 %. Further, the analytical findings will be validated through a 3D PIC code CST studio suite, in chapter 3.